Electronic Supplementary Material (ESI) for Nanoscale.

Hexa-functional Tumour Seeking Nano Voyagers and Annihilators for Synergistic Cancer Theranostic Application

Arathyram Ramachandra Kurup Sasikala [1, 2#], Afeesh Rajan Unnithan [1, 2#], Reju George Thomas[3], Tumurbaatar Batgerel [1,4], Yong Yeon Jeong[3], Chan Hee Park[1, 2*], Cheol Sang Kim [1, 2*]*

(# both authors contributed equally to the work)

[1]Dr. Arathyram Ramachandra Kurup Sasikala, Dr. Afeesh Rajan Unnithan, Prof. Chan Hee Park, Prof. Cheol Sang Kim, Department of Bionanosystem Engineering, Graduate School, Chonbuk National University, Jeonju 561-756, Republic of Korea

[2] Dr. Arathyram Ramachandra Kurup Sasikala, Dr. Afeesh Rajan Unnithan , Prof Chan Hee Park, Prof. Cheol Sang Kim, Mechanical Design Engineering, Chonbuk National University, Jeonju 561-756, Republic of Korea

[3] Reju George Thomas, Yong Yeon Jeong, Department of Radiology, Chonnam National University Hwasun Hospital, Hwasun 58128, Biomolecular Theranostics (BiT) Lab, South Korea

[4]Power Engineering School, Mongolian University of Science and Technology, Ulaanbaatar, Mongolia

Magnetic property measurement and *in vitro* thermal characteristics

Magnetic properties of the as prepared IONPs and MMGCPTs were analyzed by measuring the magnetization as a function of the applied magnetic field at 300K (Figure S4A). The hysteresis loops of IONPs and MMGCPTs clearly indicate the superparamagnetic behavior by exhibiting no coercivity or remanence with a high saturation magnetization of 87.79 emu/g and 74.34 emu/g, respectively.

The magnetic field-dependent heating ability of was measured using an alternating magnetic field generator (OSH-120-B, OSUNG HITECH, Republic of Korea). In a typical experiment, the IONPs at various concentrations was placed on the center of a water-cooled induction coil made of copper connected with the AMF generator and the strength and frequency of the magnetic fields were adjusted to 12.57 kA/m and 293 kHz, respectively. The heating characteristics and the corresponding thermal images were monitored real time using NEC thermal camera TS9230. It has been found that the nanoparticle exhibits a very good hyperthermic capability at a concentration greater than 1mg/ml (Figure S2B). The same procedure has been carried out to evaluate the AMF induced heating ability of MMGCPT.

The photothermal properties of MMGCPT were studied using a near infrared continuous laser at 808 nm. For that, the samples were first placed in the holder and then illuminated by the laser ($1W/cm^2$) and the temperature elevation was recorded using the same procedure as in HT. The heating characteristics of MMGCPT for magnetophotothermia were also carried out according to the same procedure by simultaneous application of AMF and laser.

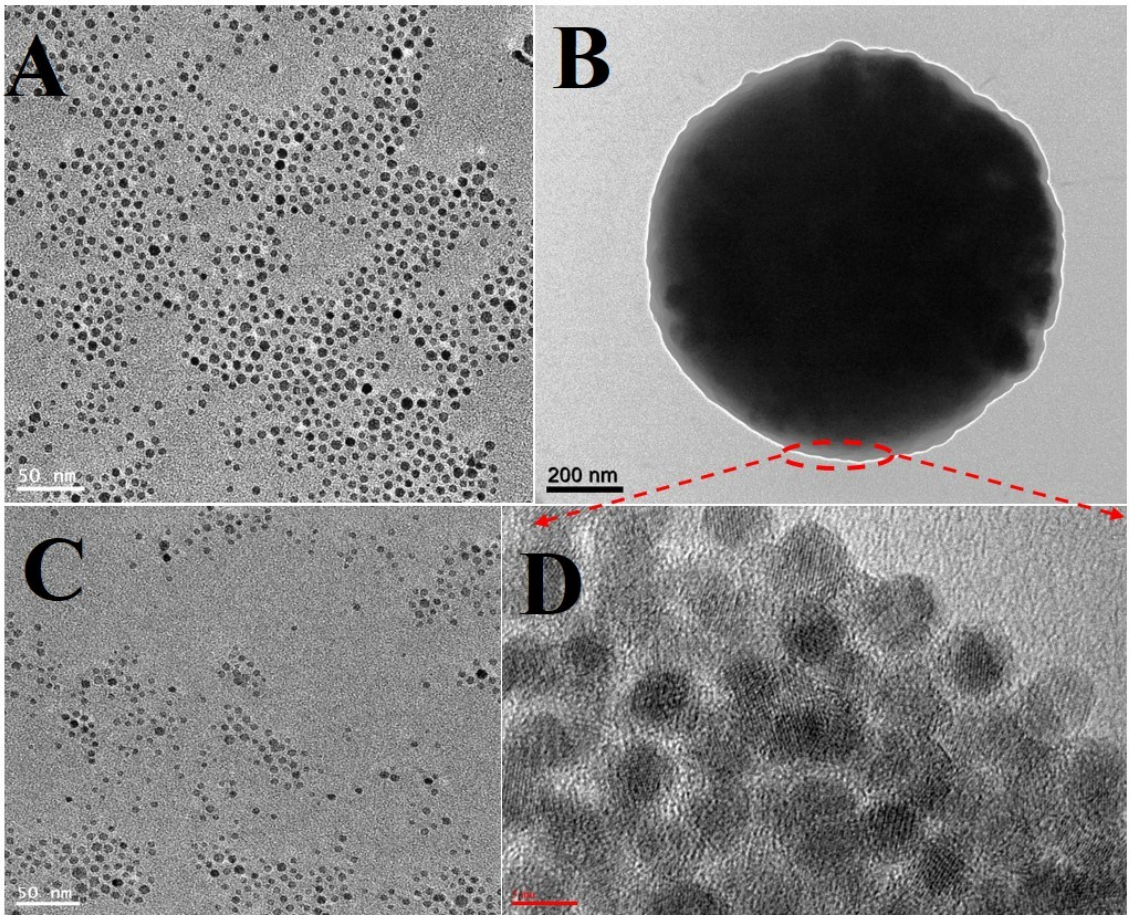

Figure S1. HR TEM image showing A) the SPIONs before loading in to MMGCPT A) at low magnification, B) Bio TEM image of MMGCPT, C) HR TEM image of the released SPIONs from MMGCPT, D) HR TEM image showing the encapsulated SPION within MMGCPT without agglomeration.

In order to check the entrapment efficiency of PTX on to the MMGCPT different feed ratio of MMGC: PTX was taken starting from 1 mg, 3 mg and 6mg of PTX to fixed (10 mg) MMGC and the entrapment efficiency was calculated using the following equation

$$\%\ Entrapment\ efficiency = \frac{Initial\ concentration\ of\ drug - Drug\ content\ in\ the\ supernatant}{Initialconcentration\ of\ drug}\ x\ 100$$

The results were given below. It has been found that, a feed ratio of 10: 3 (MMGC: PTX), exhibited an enhanced entrapment efficiency of 60.6%.

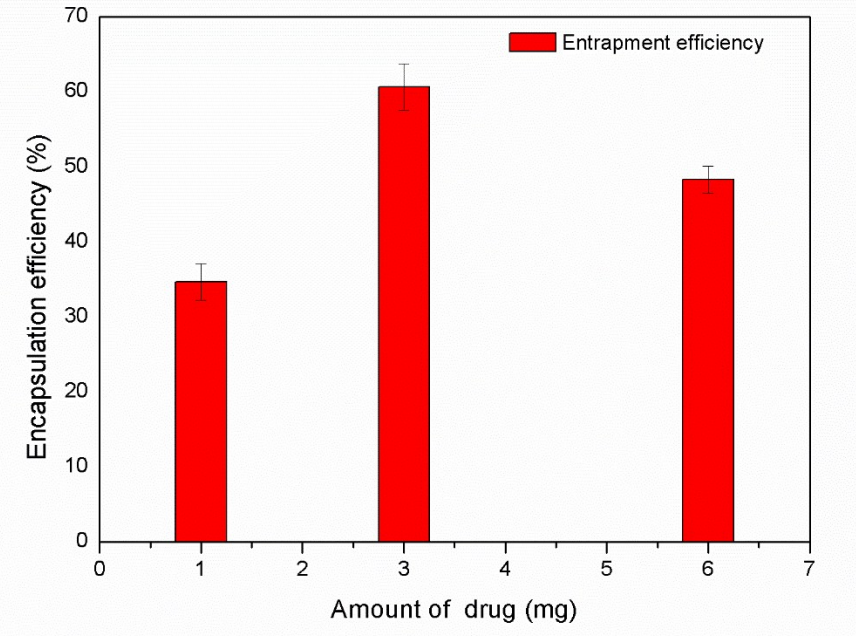

Figure S2. Entrapment efficiency of MMGCPT at different concentration of PTX

The loading efficiency of SPIONs inside the micelle was determined using the TGA analysis. The SPIONs alone didn't show any significant degradation profile as SPIONs are unaffected by the higher temperature. At the same time, the TGA data of the MMGCPT showed a clear weight loss profile after the experiment. The weight loss observed for the MMGCPT were attributed to the decomposition of HGC micelle around the SPIONs. It is shown that the percentage residual weight for MMGCPT is 83.43% which is the estimated amount of IONPs taken up by the micelle during the present experiment as shown in the figure S3.

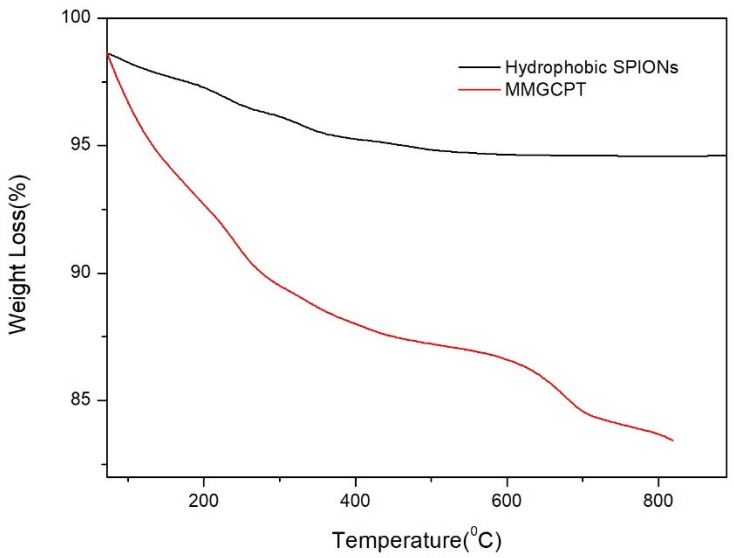

Figure S3. TGA profile of MMGCPT and SPIONs

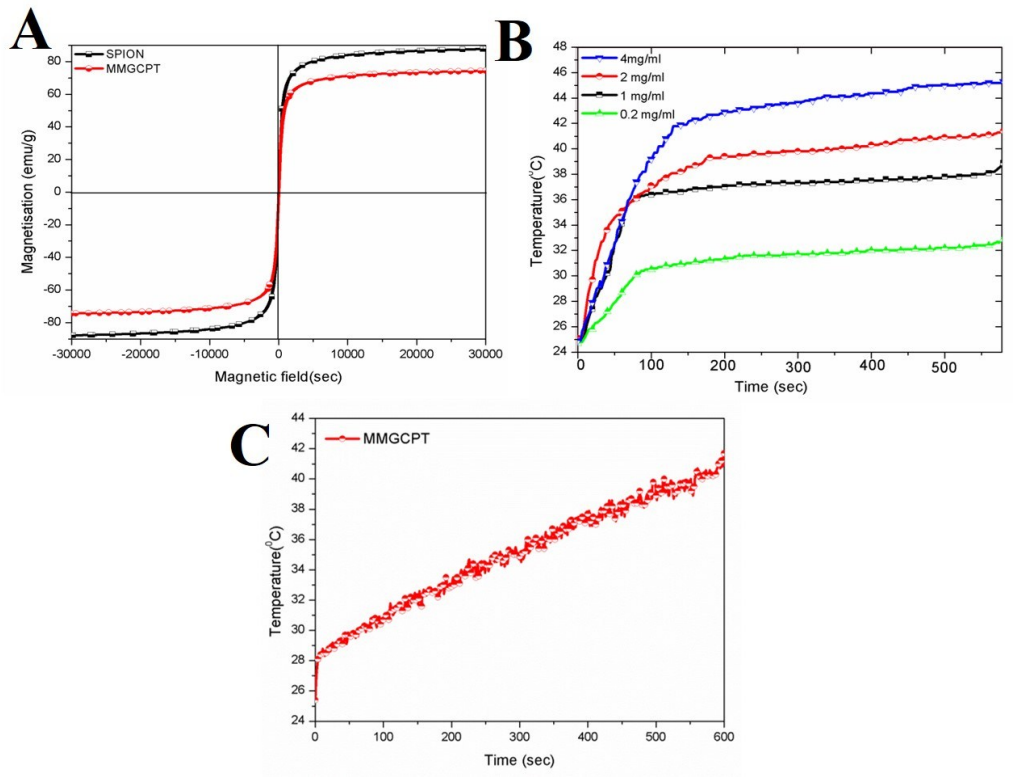

Figure S4. A) Magnetic hysteresis curve of SPIONs and MMGCPT, B) Heating ability of SPIONs under AMF application, C) AMF induced heating ability of MMGCPT.

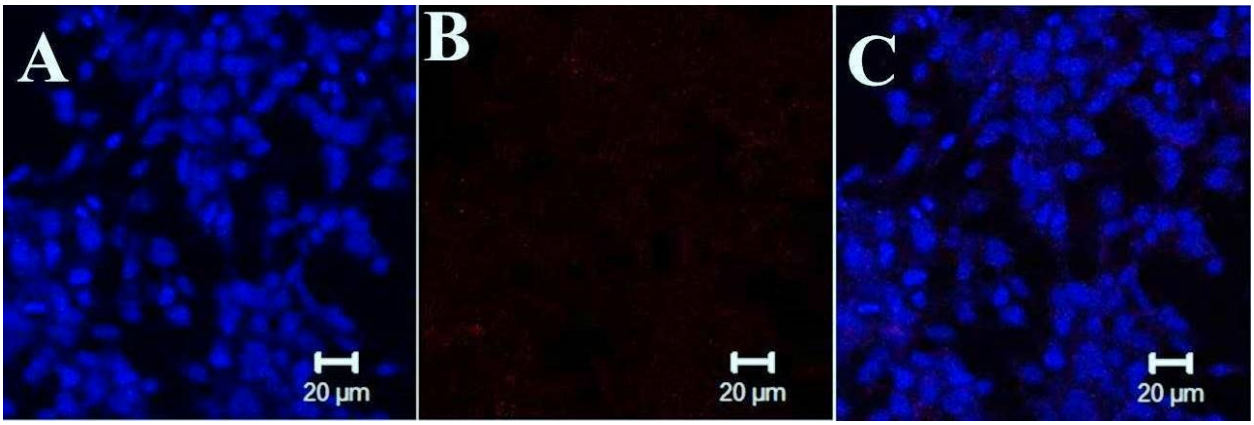

Figure S5. CLSM showing the selective uptake of MMGC by cancer cells compared to normal cells (NIH3T3): A) DAPI, B) NIR (no red fluorescence due to the lack of MMGC uptake) and C) Merge.

The system design and morphological operation employed for the deep learning method to detect the tumor cell nuclei is outlined below.

Create the dataset:

It is the first step, here we insert the original image file (H&E image) and is read with IMAQ function and image processing concepts in LabVIEW. The IMAQ palette helps to make the system straight-forward and intuitive to perform the image processing and analysis required for the simulation.

Convert images to train:

Dataset is then used to train the artificial neural network. This is done in MATLAB, as the complex program that trains the artificial neural network was inherited from the programing through to a Math-Script node and then it is passed to LabVIEW

A double threshold is performed on the image and all pixels with intensities between 0 and "Grayscale threshold" become pure black. All pixels with intensities between Grayscale threshold increase one by one (++1) and 255 become pure white. A histogram count and graphs the total number of pixels at each grayscale level.

The particles that touch the boarder of the images is removed and filtered out with an area less than 50 pixels. So, the rest of the analysis is done only if there are less than 100 particles in the image. Predict the value of each digit in the test set and create a 20x20 pixel image out of each region of interest (ROI) and build a single ROI descriptor from an array of descriptors. Each 20x20 image contains one and only one type area.

The 20x20 pixel images are converted to numeric 2D arrays with 20 rows and 20 columns. The 20x20 2D arrays are flattened into 400xI vectors. Each such vector contains the information for one (cancer cell) colour area.

Training the artificial intelligent network and deep learning method:

It consists of an input layer, several hidden layers, and an output layer. The layers are interconnected via nodes or neurons with each hidden layer using the output of the previous layer as its input.

Input layer: 20x20 pixels and 400 cell image input, Hidden layer: acceptable term image analysis patch, predict the value of each object in the test set, Output layer: Overlay the predicted values and confidence level. Using the training data, the network starts to understand the object's specific features and associate them with the corresponding category. Each layer in the network takes in data from the previous layer, transforms it and passes it on. The network increases the complexity and detail of what it is learning from layer to layer. Figure S4 A, gives an overall idea of the neural network and Figure S4 B, gives the overall idea of the proposed deep learning-based cancer cell nuclei detection method.

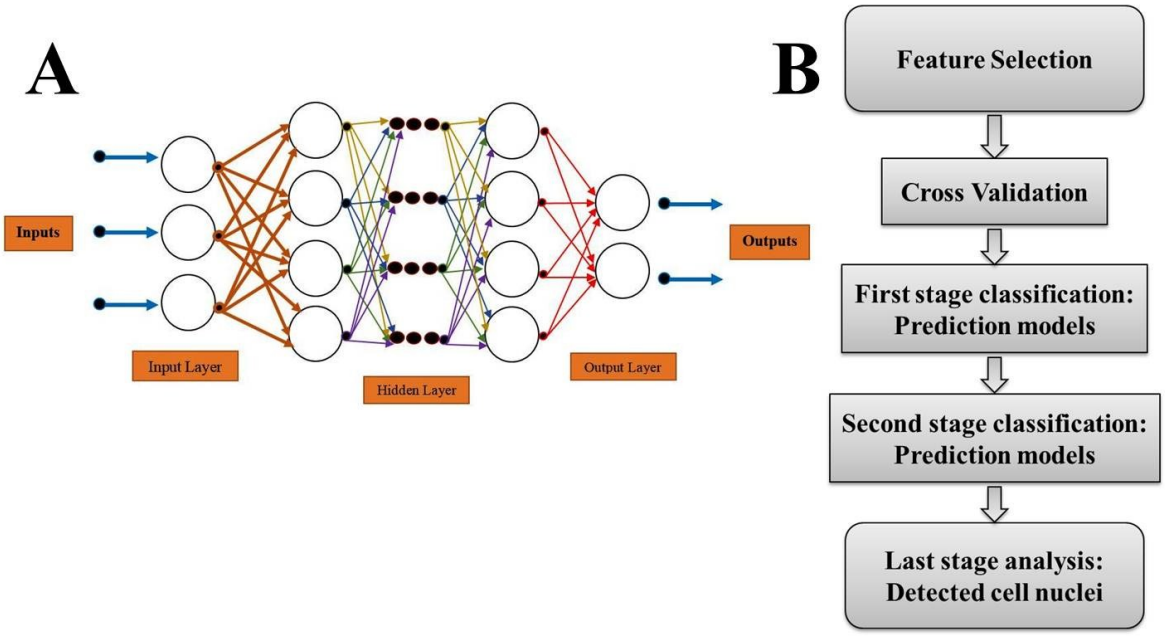

Figure S6. A) An illustration of the neural network employed in the present study, B) Flowchart of the proposed deep learning-based cancer cell nuclei detection method.